CHAPTER 1

Introduction

Condensed information storage in miniature computers, infinitesimal machinery for space exploration, microscopic surgical tools, and modern telecommunications are only a few of the vast number of applications that lie at the roots of microsystem technology. Richard Feynman may not have been the only one to anticipate the need to develop this important area of modern technology, but he is definitely one of the pioneers in describing possible ways of locomotion for such microdevices, by advocating for techniques and ideas based on fundamental principles of physics, chemistry, and biology, and ranging from electrostatic actuation to quantum computation at the atomic electron levels [**68, 69**].

Microelectromechanical systems (MEMS) and *nanoelectromechanical systems* (NEMS) are now a well-established sector of contemporary technology. A comprehensive overview of their rapidly developing field can be found in the relatively recent monograph of Pelesko and Bernstein [**140**], which is a good source of information about the various areas of applications of MEMS. It also contains justifications and derivations of the fundamental partial differential equations that model such devices. More complicated models have also been proposed by E. M. Abdel-Rahman, M. I. Younis, and A. H. Nayfeh (see, for example, [**1, 137, 162**]).

It is the mathematical analysis of some of these equations that concerns us in this monograph. We shall therefore settle in this introduction on a quick derivation of one of the most basic PDEs modeling electrostatic MEMS devices, and then proceed towards stating some of the problems that interest applied analysts and engineers, while giving some numerical and heuristic evidence for various conjectures that will be addressed rigorously throughout this book.

1.1. Electrostatic Actuations and Nonlinear PDEs

A key component of some MEMS systems is the simple idealized electrostatic device shown in Figure 1.1. The upper part of this device consists of a thin and deformable microplate that is held fixed along its boundary $\partial\Omega$, where Ω is a bounded domain in $\mathbb{R}^2$. The dielectric elastic microplate lies above a parallel rigid grounded plate, say at level $z = -d$, and has an upper surface that is coated with a negligibly thin metallic conducting film. When a voltage V is applied to the conducting film, it deflects towards the bottom plate, and if the applied voltage V is increased beyond a certain critical value V^*, then the mechanical forces defined by the deformable plate can no longer resist the opposing electrostatic force, thereby leading it to touch the grounded plate. The steady state of the system is then lost, and we have a snap-through at a finite time creating the so-called pull-in instability.

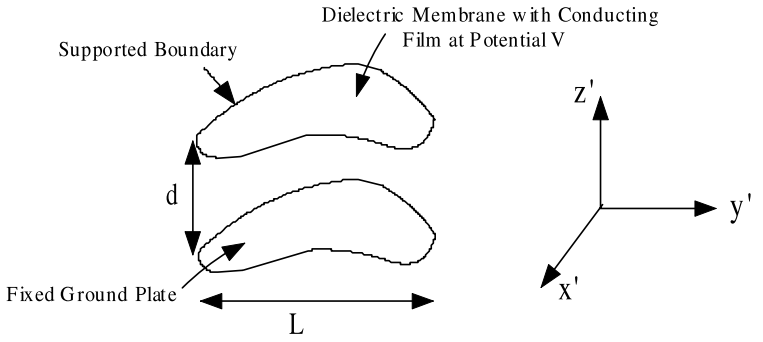

FIGURE 1.1. The simple electrostatic MEMS device.

A mathematical model of this physical phenomenon when the plate is one dimensional, i.e., a beam of length L, already leads to the following interesting partial differential equation for its dimensionless dynamic deflection:

$$\frac{\partial^2 u}{\partial t^2} + a\frac{\partial u}{\partial t} = (\alpha_1 \|u_x\|_2^2 + T)\frac{\partial^2 u}{\partial x^2} - B\frac{\partial^4 u}{\partial x^4} - \frac{\alpha_2 f(t)^2}{(d+u)^2},$$
$$u(0,t) = u(L,t) = 0, \quad \frac{\partial u}{\partial x}(0,t) = \frac{\partial u}{\partial x}(L,t) = 0,$$

which was already derived by several authors. All the constants above—a, α_1, T, B, and α_2—are assumed to be nonnegative. See for example, the survey paper of Marquès-Castello-Shkel [**63**], Pelesko-Bernstein [**140**], or [**20, 73, 152**] and the references therein.

The case of a capacitively actuated, two-dimensional microplate is much more complicated as described by Nayfeh et al. in [**137**], especially if one accounts for moderately large deflections, since one needs to use the dynamic analogue of the von Kármán equations. We shall therefore only consider the case where the deformations are small, so that each material point moves vertically over its reference position, and so that the material response is essentially linear. In this case the dynamic deflection $u = u(x,t)$ of the membrane on a bounded domain Ω in $\mathbb{R}^2$ is assumed to satisfy the following evolution equation:

$$\rho A\frac{\partial^2 u}{\partial t^2} + a\frac{\partial u}{\partial t} = T\Delta u - B\Delta^2 u - \frac{C^2V^2}{(d+u)^2} \quad \text{for } x \in \Omega, t > 0, \tag{1.1a}$$

$$-1 < u(x,t) \le 0 \quad \text{for } x \in \Omega, t > 0, \tag{1.1b}$$

$$u(x,t) = B\frac{\partial u}{\partial \eta}(x,t) = 0 \quad \text{for } x \in \partial\Omega, t > 0, \tag{1.1c}$$

$$u(x,0) = 0 \quad \text{and} \quad u_t(x,0) \ge 0 \quad \text{for } x \in \Omega, \tag{1.1d}$$

where $\Delta^2 := -\Delta(-\Delta\,\cdot)$ denotes the biharmonic operator, η denotes the outward pointing unit normal to $\partial\Omega$, and

- ρ is the mass density per unit volume of the membrane and A is its thickness,
- a is a damping intensity,
- T is the tension constant in the stretching component of the energy,
- B accounts for the bending energy and is given by $B = \frac{2A^3Y}{3(1-\nu^2)}$ where Y is the Young modulus and ν is the Poisson ratio,
- the uniformly distributed charges over the membrane and the bottom plate are subjected to a capacitive influence of capacitance C and a fixed electric voltage V,
- the initial condition in (1.1d) assumes that the membrane is initially undeflected and the voltage is suddenly applied to the upper surface of the membrane at time $t = 0$,
- the boundary condition (1.1c) reflects the fact that the membrane is held fixed along its boundary $\partial\Omega$ on the level $z = 0$.

Even then we have neglected several factors in the system. Indeed, while we include an external viscous damping (linked to air friction), we have disregarded internal structural damping generated by the molecular interaction in the material due to deformations; see [**63**]. We have also assumed the tension to be constant by considering only a small aspect ratio $\frac{d}{L} \ll 1$.

There are several issues that must be considered in the actual design of MEMS devices. Typically one of the primary goals is to achieve the maximum possible stable deflection before touchdown occurs, which is referred to as pull-in distance (cf. [**99, 139**]). Another consideration is to increase the stable operating range of the device by improving the pull-in voltage V^* subject to the constraint that the range of the applied voltage is limited by the available power supply. Such improvements in the stable operating range are important for the design of certain MEMS devices, such as microresonators. One way of achieving larger values of V^* while simultaneously increasing the pull-in distance consists of introducing a spatially varying dielectric permittivity $\varepsilon_2(x)$ of the membrane. We shall see in Section 1.3 that the equation becomes of the form

$$\rho A\frac{\partial^2 u}{\partial t^2} + a\frac{\partial u}{\partial t} = T\Delta u - B\Delta^2 u - \frac{\lambda\varepsilon_0}{\varepsilon_2(x)(d+u)^2} \quad \text{for } x \in \Omega,\ t > 0, \tag{1.2}$$

where ε_0 is the permittivity of free space, and λ is a positive constant that is proportional to the square of the supply voltage.

In other situations, cf. [**140, 141, 142**], the capacitance C of the actuator may depend on the deformation variable u according to the relation

$$C = \gamma \int_\Omega \frac{1}{d+u(x)}\,dx. \tag{1.3}$$

As a result, the voltage drop V at the actuator can no longer be kept at the constant supply voltage V_s, but is instead given by the series circuit formula $V = \frac{V_s}{(1+C/C_f)}$ where C_f is the circuit series capacitance. Therefore, in view of (1.3), V depends

on the deformation variable u according to

$$V = \frac{V_s}{(1 + \xi \int_\Omega \frac{1}{d+u(x)}\, dx)},$$

where $\xi = \frac{\gamma}{C_f}$ reflects the influence of the circuit series capacitance, and we eventually arrive at the nonlocal equation

$$\rho A \frac{\partial^2 u}{\partial t^2} + a\frac{\partial u}{\partial t} = T\Delta u - B\Delta^2 u - \frac{\lambda}{(d+u)^2(1 + \xi \int_\Omega \frac{1}{d+u(x)}\, dx)^2}, \tag{1.4}$$

where $\lambda = C^2 V_s^2 > 0$ is a constant that is proportional to the square of the supply voltage V_s.

1.2. Derivation of the Model for Homogeneous Systems

A typical MEMS device is subject to electrostatic, elastic, and dynamic forces. We first deal with the case of a membrane with constant permittivity profile.

1.2.1. Analysis of the Simplified Electrostatic Problem. The Coulomb law states that the electrostatic force F between two charges q_1 and q_2 placed at a distance r apart is given in normalized units by

$$F = \frac{q_1 q_2}{r^2}.$$

If the two charges are uniformly distributed over two parallel plates subject to a capacitive influence of capacitance C and a fixed electric voltage V, then we can write q_1 and q_2 as $q_1 = q = CV = -q_2$ and F becomes $F = -C^2V^2/r^2$. If now one of the plates stretches a small vertical distance dr, then the work done is $F\, dr$, which decreases the electric potential stored in the capacitor. As a consequence, the electric potential W can be expressed as

$$W = -\frac{C^2V^2}{r}. \tag{1.5}$$

In the more general situation, when the electric charges are not uniformly distributed as a result of a varying distance $r = 1 + u(x)$, where $d = 1$ is the distance between the two plates in the absence of plate deformation, and $u(x)$ is the plate deformation variable, the electric potential (1.5) becomes

$$E_W(u) = -\int_\Omega \frac{C^2V^2}{1+u(x)}\, dx, \tag{1.6}$$

where Ω is the domain in $\mathbb{R}^2$ limiting the membrane.

1.2.2. Analysis of Elastic Forces. On the other hand, in the presence of a plate deformation characterized by $u \neq 0$, the elastic energy has two components: the stretching energy sector given by

$$E_S(u) = \int_\Omega \frac{T}{2}|\nabla u|^2\,dx, \tag{1.7}$$

where $T > 0$ is the tension constant, and the bending energy given by

$$E_B(u) = \int_\Omega \frac{B}{2}(\Delta u)^2\,dx, \tag{1.8}$$

where $B = \frac{2A^3Y}{3(1-\nu^2)}$, in which A is the plate thickness, Y is the Young modulus, and ν is the Poisson ratio.

Indeed, the stretching energy in the elastic membrane is proportional to the changes in the area of the membrane from its unstretched configuration. Since we assume the membrane is held fixed at its boundary, we may then write it as

$$\text{stretching energy} := T\int_\Omega \sqrt{1+|\nabla u|^2}\,dx, \tag{1.9}$$

where the proportionality constant T is simply the tension in the membrane. Our expression for E_S is then nothing but the linearization of the stretching energy. On the other hand, the bending energy is assumed to be proportional to the linearized curvature of the membrane, hence the expression for E_B, where the constant B is the flexural rigidity of the membrane.

Consequently, the total energy $E = E_S + E_B + E_W$ may be represented as

$$E(u) = \int_\Omega \left\{\frac{T}{2}|\nabla u|^2 + \frac{B}{2}|\Delta u|^2 - \frac{C^2V^2}{1+u}\right\} dx, \tag{1.10}$$

so that its Euler-Lagrange equation is

$$T\Delta u - B\Delta^2 u - \frac{C^2V^2}{(1+u)^2} = 0 \quad \text{in } \Omega. \tag{1.11}$$

1.2.3. Analysis of the Dynamic Problem. For the dynamic deflection $u(x,t)$ of the membrane, we use Newton's second law to write

$$\rho A\frac{\partial^2 u}{\partial t^2} = \sum \text{forces}, \tag{1.12}$$

where ρ is the mass density per unit volume of the membrane and A is its thickness. As to the forces, we combine the superposition of the elastic and electrostatic forces assembled in (1.11) with a damping force F_d that is linearly proportional to the velocity, that is,

$$F_d = -a\frac{\partial u}{\partial t}. \tag{1.13}$$

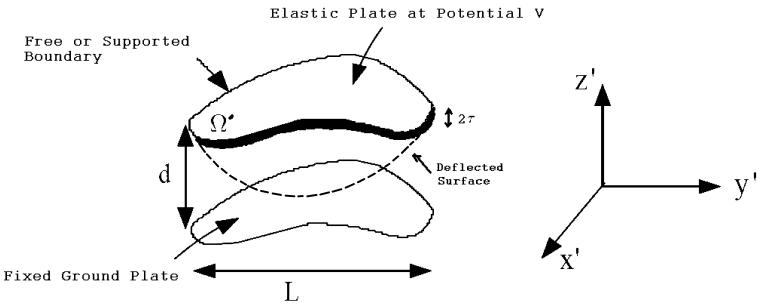

FIGURE 1.2. The key component of an electrostatic MEMS.

We finally obtain the equation

$$\rho A \frac{\partial^2 u}{\partial t^2} = -a\frac{\partial u}{\partial t} + T\Delta u - B\Delta^2 u - \frac{C^2V^2}{(1+u)^2}. \tag{1.14}$$

1.3. MEMS Models with Variable Permittivity Profiles

We now allow the elastic membrane to exhibit a spatial variation reflecting a varying dielectric permittivity. For that, we first need to formulate the equations governing the electrostatic field within the device components and around it.

1.3.1. Tailored Permittivity Profiles. For simplicity, we shall consider a two-dimensional case where both the membrane and the ground plate have width and length equal to L, and, in the undeformed state, are separated by a gap of length d; see Figure 1.2. We assume that the ground plate, located now at $z' = 0$, is a perfect conductor. The elastic membrane is assumed to be of uniform thickness $A = 2\tau$. The deflection of the membrane is specified by the deflection of its center plane, located at $z' = \widehat{u}(x', y')$. Hence the top surface is located at $z' = \widehat{u}(x', y') + \tau$, while the bottom of the membrane is located at $z' = \widehat{u}(x', y') - \tau$.

We assume that the elastic membrane is held at potential V, while the fixed ground plate is held at zero potential. The electrostatic potential ϕ_1 in the whole region D' between the elastic plate, the ground plate, and the lateral region surrounding the device must satisfy the Laplace equation on D', with boundary conditions $\phi_1 = 0$ on the ground plate. In other words,

$$\Delta\phi_1 = 0 \quad \text{on } D', \tag{1.15}$$

$$\phi_1(x', y', 0) = 0 \quad \text{in } \Omega'. \tag{1.16}$$

Denote by $\varepsilon_2(x', y')$ the varying permittivity of the membrane; the potential ϕ_2 inside the membrane must then satisfy

$$\nabla \cdot (\varepsilon_2 \nabla\phi_2) = 0 \quad \text{for } \widehat{u}(x', y') - \tau \le z' \le \widehat{u}(x', y') + \tau, \tag{1.17}$$

$$\phi_2(x', y', \widehat{u} + \tau) = V \quad \text{in } \Omega'. \tag{1.18}$$

At the interface between the gap and the membrane, the potential and the displacement fields must be continuous; hence we impose

$$\phi_1(x', y', \widehat{u}(x', y') - \tau) = \phi_2(x', y', \widehat{u}(x', y') - \tau), \tag{1.19}$$

and

$$\varepsilon_2(x', y')\nabla\phi_2 \cdot \mathbf{n} = \varepsilon_0 \nabla\phi_1 \cdot \mathbf{n} \quad \text{at } z' = \widehat{u}(x', y') - \tau, \tag{1.20}$$

where ε_0 is the permittivity of free space and $\mathbf{n}$ is an outward unit normal.

Now, introduce dimensionless variables

$$\psi_1 = \frac{\phi_1}{V}, \quad \psi_2 = \frac{\phi_2}{V}, \quad u = \frac{\widehat{u}}{d}, \quad x = \frac{x'}{L}, \quad y = \frac{y'}{L}, \quad z = \frac{z'}{d}, \tag{1.21}$$

to see that the electrostatic problem reduces to

$$\frac{\partial^2\psi_1}{\partial z^2} + \varepsilon^2\left(\frac{\partial^2\psi_1}{\partial x^2} + \frac{\partial^2\psi_1}{\partial y^2}\right) = 0, \quad 0 \le z \le u - \frac{\tau}{d}, \tag{1.22a}$$

$$\varepsilon_2(x, y)\frac{\partial^2\psi_2}{\partial z^2} + \varepsilon^2\left(\frac{\partial}{\partial x}\left(\varepsilon_2(x, y)\frac{\partial\psi_2}{\partial x}\right) + \frac{\partial}{\partial y}\left(\varepsilon_2(x, y)\frac{\partial\psi_2}{\partial y}\right)\right) = 0, \quad u - \frac{\tau}{d} \le z \le u + \frac{\tau}{d}, \tag{1.22b}$$

$$\psi_1 = 0 \quad \text{on the ground plate } z = 0, \tag{1.23}$$

$$\psi_2 = 1 \quad \text{on the upper membrane surface } z = u + \frac{\tau}{d}, \tag{1.24}$$

together with the continuity property of the potential and the displacement fields across $z = u - \frac{\tau}{d}$, that is,

$$\psi_1\left(x, y, u(x, y) - \frac{\tau}{d}\right) = \psi_2\left(x, y, u(x, y) - \frac{\tau}{d}\right), \tag{1.25}$$

$$\varepsilon^2(\varepsilon_2(x, y)\nabla_\perp\psi_2 - \varepsilon_0\nabla_\perp\psi_1)\nabla_\perp u = \varepsilon_2(x, y)\frac{\partial\psi_2}{\partial z} - \varepsilon_0\frac{\partial\psi_1}{\partial z} \quad \text{on the set } z = u(x, y) - \frac{\tau}{d}. \tag{1.26}$$

Here ψ, given by ψ_1, ψ_2, is the dimensionless potential scaled with respect to the applied voltage V, and $\varepsilon \equiv d/L$ is the so-called aspect ratio of the device. We are using the notation $\Delta_\perp$ to distinguish the differentiation in the domain variables $(x, y) \in \Omega$ from the differentiation in the space variables (x, y, z) in $\Omega \times \mathbb{R}$.

In general, one has little hope of finding an exact solution ψ from (1.22a)–(1.26). However, we can simplify the system by examining a restricted parameter regime. In particular, we consider the small-aspect ratio limit $\varepsilon \equiv \frac{d}{L} \ll 1$. Physically, this means that the lateral dimensions of the device in Figure 1.2 are larger compared to the size of the gap between the undeflected membrane and ground plate. In this case, equation (1.22) gives $\partial^2\psi_1/\partial z^2 = 0$ and $\partial^2\psi_2/\partial z^2 = 0$. It

follows that ψ_1 and ψ_2 are linear in z. Combined with the continuity of ψ across $z = w - \frac{\tau}{d}$, it means that there exists a function $\psi_0(x, y)$ such that

$$\psi = \begin{cases} \psi_1 = \psi_0 \frac{z}{u-\tau}, & 0 \le z \le u - \tau, \\ \psi_2 = 1 + \frac{(1-\psi_0)}{2\tau}(z - (u + \tau)), & u - \tau \le z \le u + \tau. \end{cases} \tag{1.27}$$

Now to ensure that the displacement field is continuous across $z = u - \tau$, we need from (1.26) that

$$\varepsilon_0 \frac{\partial \psi}{\partial z}\bigg|_- = \varepsilon_2(x, y) \frac{\partial \psi}{\partial z}\bigg|_+ \quad \text{on } z = u(x, y) - \frac{\tau}{d},$$

where the plus or minus signs indicate that $\frac{\partial \psi}{\partial z}$ is to be evaluated on the upper or lower side of the bottom surface $z = u - \tau$ of the membrane, respectively. This condition determines ψ_0 in (1.27)

$$\psi_0(x, y) = \left[1 + \frac{2\tau}{u(x, y) - \tau}\left(\frac{\varepsilon_0}{\varepsilon_2(x, y)}\right)\right]^{-1}. \tag{1.28}$$

From (1.27) and (1.28), we observe that the electric field in the z-direction inside the membrane is independent of z and is given by

$$\frac{\partial \psi}{\partial z} = \frac{\varepsilon_0}{\varepsilon_2(u - \tau)}\left[1 + \frac{2\tau}{u - \tau}\frac{\varepsilon_0}{\varepsilon_2}\right]^{-1} \sim \frac{\varepsilon_0}{\varepsilon_2 u} \quad \text{for } \tau \ll 1. \tag{1.29}$$

In other words, in the small-aspect ratio limit $\varepsilon \ll 1$ and for a very thin membrane $\tau \ll 1$ and a ground plate located at $z = -1$, we have that the electric field in the z-direction at any point of the membrane is given by

$$\frac{\partial \psi}{\partial z} = \frac{\varepsilon_0}{\varepsilon_2(x, y)(1 + u)}. \tag{1.30}$$

1.3.2. MEMS Models with a Varying Permittivity Profile. In cases where the membrane has a varying permittivity profile, we have in view of (1.14) the following system of equations for the membrane's deflection $\widehat{u}$ and the potential ϕ, which couples the solution of the elastic problem to the solution of the electrostatic problem

$$\rho A \frac{\partial^2 \widehat{u}}{\partial t'^2} + a \frac{\partial \widehat{u}}{\partial t'} - T\Delta_\perp \widehat{u} + B\Delta_\perp^2 \widehat{u} = -\frac{\varepsilon_2}{2}|\nabla \phi(x', y', \widehat{u})|^2. \tag{1.31}$$

We are again using the notation $\Delta_\perp$ to distinguish the Laplacian in the domain variables $(x', y') \in \Omega'$ from the Laplacian in the space variables (x', y', z') in $\Omega' \times \mathbb{R}$. The term on the right-hand side of (1.31) denotes the force on the elastic membrane induced by the electric field with potential $\phi(x', y', z')$, where ε_2 is the permittivity of the membrane. We have assumed that such a force is proportional to the norm squared of the gradient of the potential. A derivation of such source term may be found in [**114**]. Note that ϕ is coupled to the elastic problem via the boundary condition, which depends on the deformation of the membrane.

We now apply again dimensionless analysis to equation (1.31). We scale the electrostatic potential with the applied voltage V, time with a damping timescale

of the system, the x' (resp., y') variable with a characteristic length and width of the device equal to L, and z' and $\widehat{u}$ with the size of the gap d between the ground plate and the undeflected elastic membrane. So we define

$$u = \frac{\widehat{u}}{d}, \quad \psi = \frac{\phi}{V}, \quad x = \frac{x'}{L}, \quad y = \frac{y'}{L}, \quad z = \frac{z'}{d}, \quad t = \frac{Tt'}{aL^2}, \tag{1.32}$$

and substitute these into equation (1.31) to find

$$\gamma^2 \frac{\partial^2 u}{\partial t^2} + \frac{\partial u}{\partial t} - \Delta_\perp u + \delta \Delta_\perp^2 u = -\lambda \frac{\varepsilon_2}{\varepsilon_0} \left[\varepsilon^2 |\nabla_\perp \psi|^2 + \left(\frac{\partial \psi}{\partial z} \right)^2 \right] \quad \text{in } \Omega, \tag{1.33}$$

where Ω is the dimensionless domain of the elastic membrane. Here the parameter γ is defined as

$$\gamma = \frac{\sqrt{\rho T A}}{aL}, \tag{1.34}$$

while δ measures the relative importance of tension and rigidity, defined by

$$\delta = \frac{B}{TL^2}. \tag{1.35}$$

The parameter ε is the aspect ratio of the system

$$\varepsilon = \frac{d}{L}, \tag{1.36}$$

and the parameter λ is a ratio of the reference electrostatic force to the reference elastic force, defined by

$$\lambda = \frac{V^2 L^2 \varepsilon_0}{2Td^3}. \tag{1.37}$$

Therefore, in the small-aspect ratio limit $\varepsilon \ll 1$ we can use expression (1.30) for the field, and the governing equation (1.33) then reduces to

$$\gamma^2 \frac{\partial^2 u}{\partial t^2} + \frac{\partial u}{\partial t} - \Delta_\perp u + \delta \Delta_\perp^2 u = -\frac{\lambda \varepsilon_0}{\varepsilon_2(x, y)(1 + u)^2} \quad \text{in } \Omega. \tag{1.38}$$

We now call $f(x, y) = \frac{\varepsilon_0}{\varepsilon_2(x,y)}$ the *permittivity profile* of the device and λ the *applied voltage*, and we end up with

$$\gamma^2 \frac{\partial^2 u}{\partial t^2} + \frac{\partial u}{\partial t} - \Delta_\perp u + \delta \Delta_\perp^2 u = -\frac{\lambda f(x, y)}{(1 + u)^2} \quad \text{in } \Omega \times (0, +\infty). \tag{1.39}$$

Since the membrane is undeflected at the initial time, we must have $u(x, y, 0) = 0$, and since the boundary of the membrane is held fixed, we also have $u(x, y, t) = 0$ on the boundary of Ω at any time $t > 0$.

1.3.3. The Mathematical Equations under Study. The stationary state of equation (1.39) will be considered in Part III of this monograph, where we assume the deflection is upwards towards a ground plate at $z = 1$. We therefore consider the following fourth-order equation describing the deflection $u = u(x)$ of the membrane on a bounded domain Ω with a clamped boundary condition

$$(C_{\lambda,f}) \qquad \begin{cases} \Delta^2 u = \frac{\lambda f(x)}{(1-u)^2} & \text{in } \Omega, \\ 0 \le u < 1 & \text{in } \Omega, \\ u = \frac{\partial u}{\partial \eta} = 0 & \text{on } \partial\Omega, \end{cases}$$

with η being the outward pointing unit normal to $\partial\Omega$, and B and T are positive constants. We shall also consider the case of a pinned boundary, that is,

$$(P_{\lambda,f}) \qquad \begin{cases} B\Delta^2 u - T\Delta u = \frac{\lambda f(x)}{(1-u)^2} & \text{in } \Omega, \\ 0 \le u < 1 & \text{in } \Omega, \\ u = \Delta u = 0 & \text{on } \partial\Omega. \end{cases}$$

In the first part of the monograph, we shall actually consider the stationary equation in the case where the membrane is assumed to be perfectly elastic and has no rigidity, which means that $\delta = 0$ in view of (1.35). In other words, we shall focus on the familiar second-order nonlinear eigenvalue problem:

$$(S_{\lambda,f}) \qquad \begin{cases} -\Delta u = \frac{\lambda f(x)}{(1-u)^2} & \text{in } \Omega, \\ 0 \le u < 1 & \text{in } \Omega, \\ u = 0 & \text{on } \partial\Omega. \end{cases}$$

The dynamic deflection $u = u(x,t)$ will be considered in Part II, but not before we make a huge simplification to the model by ignoring rotational inertia, which would have given the equation a hyperbolic character. In other words, we assume that the membrane thickness $A = 2\tau$ is negligible, which gives $\gamma \ll 1$ in view of (1.34). We therefore end up with the following parabolic equation on a time interval $(0, T)$:

$$(D_{\lambda,f}) \qquad \begin{cases} \frac{\partial u}{\partial t} - \Delta u = \frac{\lambda f(x)}{(1-u)^2}, & (x,t) \in \Omega \times (0,T), \\ u(x,t) = 0, & (x,t) \in \partial\Omega \times (0,T), \\ u(x,0) = 0, & x \in \Omega. \end{cases}$$

We note that this type of nonlinearities (with negative exponents) have also appeared in other models, especially those concerned with the dynamics of thin films of viscous fluids; see, for example, Bertozzi, Laugesen, Pugh [**21, 22, 122, 123**] and the references therein. Earlier work dealt with the determination of the equilibrium state of two neighboring charged liquid drops suspended over two circular rings that is governed by the equation

$$\Delta v = \alpha + \frac{\beta}{v^2} \quad \text{in } \Omega, \tag{1.40}$$

where $\alpha, \beta > 0$ are constants reflecting fluid-mechanical and electrostatic properties of the drops, respectively, so that $\alpha = 0$ corresponds to the situation where

uncharged drops are flat (see Taylor [**157**] and also [**33, 113, 120, 136**]). The equations

$$\Delta v = \frac{1}{v^p} \quad 0 < p \leq 1, \tag{1.41}$$

have also been studied in the literature. The case where $p = 1$ is related to the study of singular minimal hypersurfaces with symmetry; see Meadows [**131**], Simon [**153**], and the references therein.

We shall concentrate in this monograph on the case when $p = 2$, but most of the results can be extended to more general nonlinearities of the form $F(x,u) = \frac{\lambda f(x)}{(1-u)^p}$, where $p > 0$. We encourage the interested reader to work out these extensions.

Particular attention will be given to the much less studied case of a varying permittivity profile f. Some of the results are straightforward extensions of the case where f is a constant already considered in [**26, 135**] such as the case when f is assumed to be bounded away from zero. More interesting situations deal with somewhere vanishing profiles, the easiest of which are power-law permittivities of the form $f(x) = |x|^\alpha$. We shall see that they can sometimes dramatically change the picture. We often try to cover both situations at once by considering profiles of the form

$$f(x) = \Big(\prod_{i=1}^{k} |x - p_i|^{\alpha_i} \Big) g(x), \quad g(x) \geq C > 0 \text{ in } \Omega. \tag{1.42}$$

1.4. Bifurcation Diagrams and Numerical Evidence

In order to get an initial idea of what issues need to be addressed, we start by considering the equation

$$(S_\lambda) \qquad \begin{cases} -\Delta u = \frac{\lambda}{(1-u)^2} & \text{in } \Omega, \\ 0 \leq u < 1 & \text{in } \Omega, \\ u = 0 & \text{on } \partial\Omega, \end{cases}$$

where Ω is the unit ball $B_1(0) \subset \mathbb{R}^N$ $(N \geq 1)$. In this case, (S_λ) possesses only radially symmetric solutions [**85**], in which case the equation reduces to

$$\begin{cases} -u_{rr} - \frac{N-1}{r} u_r = \frac{\lambda}{(1-u)^2}, & 0 < r \leq 1, \\ u'(0) = 0, & u(1) = 0. \end{cases} \tag{1.43}$$

Here $r = |x|$ and $0 < u = u(r) < 1$ for $0 < r < 1$. This problem was studied in depth by Joseph-Lundgren [**116**]. The ODE analysis of (S_λ) points to a set of solutions that varies considerably with the dimension. It is illustrated in the bifurcation diagram Figure 1.3, which describes the graph

$$G = \{(\lambda, u(0)) \in (0, +\infty) \times [0,1) : u \text{ is a solution of } (S_\lambda)\}. \tag{1.44}$$

Note that in this case, the maximum of a solution u necessarily occurs at the origin [**79**]. This diagram suggests the following structure for the solution set in more

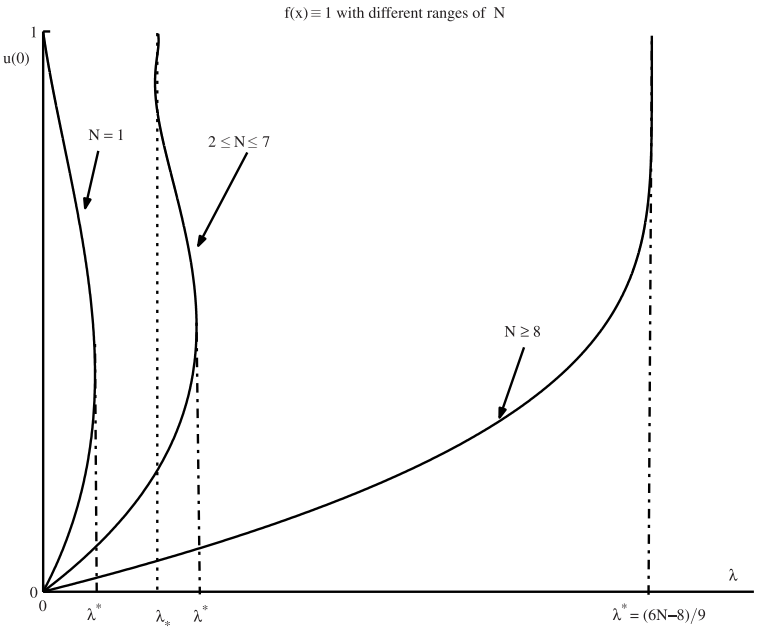

FIGURE 1.3. Plots of $u(0)$ versus λ for profile $f(x) \equiv 1$ defined in the unit ball $B_1(0) \subset \mathbb{R}^N$ with different ranges of N.

general domains Ω and permittivity profiles f, and a substantial part of this monograph investigates the extent to which these properties of the global set of solutions can be established mathematically in more general situations. Here are some of the issues that we address.

I. Estimate the *pull-in voltage* $\lambda^*(\Omega, f)$, which is the parameter $\lambda^* > 0$ such that $(S_{\lambda,f})$ has at least one solution if $\lambda < \lambda^*$, while it has none if $\lambda > \lambda^*$. What is the effect of the geometry of the domain and the permittivity profile on the value of $\lambda^*(\Omega, f)$?

II. In dimension 1, there exist exactly two branches of solutions for $0 < \lambda < \lambda^*$, and one solution for $\lambda = \lambda^*$. The bifurcation diagram disappears (goes back to $(0, 1)$) when it returns to $\lambda = 0$.

III. For dimensions $2 \le N \le 7$, there exists a curve $(\lambda(t), u(t))_{t \ge 0}$ in the solution set

$$\mathcal{V} = \{(\lambda, u) \in (0, +\infty) \times C^1(\bar{\Omega}) : u \text{ is a solution of } (S_{\lambda,f})\} \tag{1.45}$$

starting from $(0, 0)$ at $t = 0$ and going to "infinity": $\|u(t)\|_\infty \to 1$ as $t \to +\infty$, with infinitely many bifurcation or turning points in $\mathcal{V}$.

IV. In dimension $N \ge 2$ and for any profile f, there exists a unique solution for small voltages λ.

V. There is at most one solution at λ^*—the so-called extremal solution u^*—and in dimensions $2 \le N \le 7$, there exist exactly two solutions for λ in a small left neighborhood of λ^*.

VI. Estimate the *pull-in distance*, which is the maximum of the extremal solution at λ^* (i.e., $\|u^*\|_\infty$) in terms of the geometry of the domain and the permittivity profile f.

1.4.1. Bifurcation Diagrams for Power-Law Profiles. By carrying out the analysis of Joseph and Lundgren for radially symmetric solutions, but in the case of a power-law permittivity profile $f(x) = |x|^\alpha$, that is for

$$(S_{\lambda,\alpha}) \qquad \begin{cases} -\Delta u = \frac{\lambda |x|^\alpha}{(1-u)^2} & \text{in } \Omega, \\ 0 \le u < 1 & \text{in } \Omega, \\ u = 0 & \text{on } \partial\Omega, \end{cases}$$

where Ω is the unit ball $B_1(0) \subset \mathbb{R}^N$, one can already see a much richer situation induced by the nonconstant profile. We shall do that, so as to present analytical and numerical evidence for various conjectures relating to these profiles, some of which will be further discussed and proved for general domains in the next chapters. In this case, $(S_{\lambda,\alpha})$ for radially symmetric solutions reduces to

$$\begin{cases} -u_{rr} - \frac{N-1}{r} u_r = \frac{\lambda r^\alpha}{(1-u)^2}, \quad 0 < r \le 1, \\ u'(0) = 0 = u(1). \end{cases} \tag{1.46}$$

Equivalently, we can consider the initial value problem

$$\begin{cases} U'' + \frac{N-1}{r} U' = \frac{r^\alpha}{U^2}, & r > 0, \\ U'(0) = 0, & U(0) = 1. \end{cases} \tag{1.47}$$

Observe that $U > 1$ in $(0, +\infty)$. For any $\gamma > 0$, we can define a solution $u_\gamma(r)$ of (1.46) as

$$u_\gamma(r) = 1 - \lambda^{\frac{1}{3}} \gamma^{-\frac{2+\alpha}{3}} U(\gamma r).$$

The parameter λ and the maximum value $u_\gamma(0)$ of u_γ depend on γ in the following way:

$$\begin{cases} u_\gamma(0) = 1 - \frac{1}{U(\gamma)}, \\ \lambda = \frac{\gamma^{2+\alpha}}{U^3(\gamma)}, \end{cases} \tag{1.48}$$

where the second relation guarantees the boundary condition $u_\gamma(1) = 0$.

One can numerically integrate the initial value problem (1.47) and use the results to compute the complete bifurcation diagram for (1.46). We show such a computation of $u(0)$ versus λ defined in (1.48) for the slab domain ($N = 1$) in Figure 1.4. In this case, one observes from the numerical results that when $N = 1$ and $0 \le \alpha \le 1$, there exist exactly two solutions for $(S_{\lambda,\alpha})$ whenever $\lambda \in (0, \lambda^*)$. On the other hand, the situation becomes more complex for $\alpha > 1$ as $u(0) \to 1$. This leads to the question of determining the asymptotic behavior of $U(r)$ as $r \to \infty$. Towards this end, we proceed as follows:

Setting $v(s) = r^{-(2+\alpha)/3} U(r) > 0$, $r = e^s$, we have that

$$v'' + \left(N - \frac{2}{3} + \frac{2\alpha}{3} \right) v' + \frac{2+\alpha}{3} \left(N - \frac{4}{3} + \frac{\alpha}{3} \right) v = v^{-2}. \tag{1.49}$$

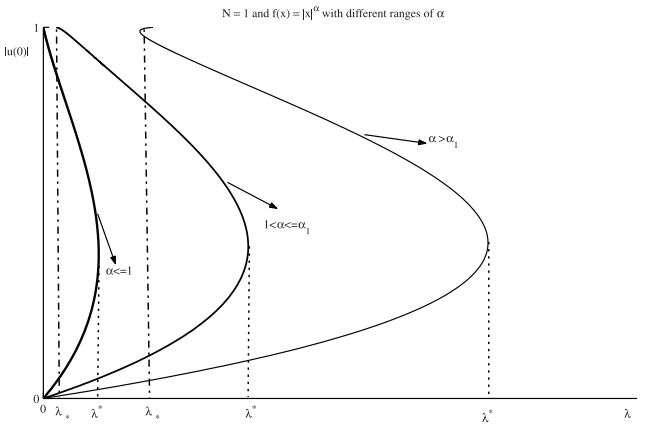

FIGURE 1.4. Plots of $u(0)$ versus λ for profile $f(x) = |x|^\alpha$ ($\alpha \geq 0$) defined in the slab domain ($N = 1$). The numerical experiments point to a constant $\alpha_1 > 1$ (analytically given in (1.50)) such that the bifurcation diagrams are greatly different for different ranges of α: $0 \leq \alpha \leq 1$, $1 < \alpha \leq \alpha_1$, and $\alpha > \alpha_1$.

We can already id entify from this equation the following regimes:

Case 1. Assume that $N = 1$ and $0 \leq \alpha \leq 1$.

In this case, there is no positive equilibrium point for (1.49), which means that the bifurcation diagram disappears at $\lambda = 0$. Then one infers that there exist exactly two solutions for $\lambda \in (0, \lambda^*)$ and just one for $\lambda = \lambda^*$.

Case 2. N and α satisfy either one of the following conditions: $N = 1$ and $\alpha > 1$, or $N \geq 2$.

There exists then a positive equilibrium point v_e of (1.49),

$$v_e = \sqrt[3]{\frac{9}{(2+\alpha)(3N+\alpha-4)}} > 0.$$

Linearizing around this equilibrium point by writing

$$v = v_e + \delta e^{\sigma\eta}, \quad 0 < \delta \ll 1,$$

we obtain that

$$\sigma^2 + \frac{3N+2\alpha-2}{3}\sigma + \frac{(2+\alpha)(3N+\alpha-4)}{3} = 0.$$

Such an equation admits the following solutions:

$$\sigma_\pm = -\frac{3N+2\alpha-2}{6} \pm \frac{\sqrt{\Delta}}{6},$$

with

$$\Delta = -8\alpha^2 - (24N-16)\alpha + (9N^2 - 84N + 100).$$

We note that $\sigma_\pm < 0$ whenever $\Delta \geq 0$. Now define

$$\alpha_1 = -\frac{1}{2} + \frac{3}{4}\sqrt{6}, \quad \alpha_N = \frac{3N - 14 - 4\sqrt{6}}{4 + 2\sqrt{6}} \quad (N \geq 8). \tag{1.50}$$

Next, we discuss the ranges of N and α such that $\Delta \geq 0$ or $\Delta < 0$.

Case 2A. N and α satisfy one of the following two conditions:

$$N = 1 \quad \text{with } 1 < \alpha \leq \alpha_1, \tag{1.51a}$$

$$N \geq 8 \quad \text{with } 0 \leq \alpha \leq \alpha_N. \tag{1.51b}$$

In this case, we have $\Delta \geq 0$ and

$$v(s) \sim \left(\frac{9}{(2+\alpha)(3N+\alpha-4)}\right)^{\frac{1}{3}} + \delta_1 e^{-\frac{3N+2\alpha-2-\sqrt{\Delta}}{6}s} + \cdots \quad \text{as } s \to +\infty.$$

Further, we conclude that

$$U(r) \sim r^{\frac{2+\alpha}{3}}\left(\frac{9}{(2+\alpha)(3N+\alpha-4)}\right)^{\frac{1}{3}} + \delta_1 r^{-\frac{N-2}{2}+\frac{\sqrt{\Delta}}{6}} + \cdots \quad \text{as } r \to +\infty.$$

In both cases, the branch monotonically approaches the value 1 as $\gamma \to +\infty$ ($u_\gamma(0) \uparrow 1$ as $\gamma \to +\infty$). Moreover, since $\lambda = \gamma^{2+\alpha}/U^3(\gamma)$, we have

$$\lambda \uparrow \lambda_* = \frac{(2+\alpha)(3N+\alpha-4)}{9} \quad \text{as } \gamma \to \infty, \tag{1.52}$$

which is an important critical threshold for the voltage. In the case (1.51a) illustrated by Figure 1.4, we have $\lambda_* < \lambda^*$, and the number of solutions increases but remains finite as λ approaches λ_*. On the other hand, in the case of (1.51b) illustrated by Figure 1.5(b), we have $\lambda_* = \lambda^*$, and there seems to be only one branch of solutions.

Case 2B. N and α satisfy one of the following conditions:

$$N = 1 \quad \text{with } \alpha > \alpha_1, \tag{1.53a}$$

$$2 \leq N \leq 7 \quad \text{with } \alpha \geq 0, \tag{1.53b}$$

$$N \geq 8 \quad \text{with } \alpha > \alpha_N. \tag{1.53c}$$

In this case, we have $\Delta < 0$ and

$$v(s) \sim \left(\frac{9}{(2+\alpha)(3N+\alpha-4)}\right)^{\frac{1}{3}} + \delta_1 e^{-\frac{3N+2\alpha-2}{6}s}\cos\left(\frac{\sqrt{-\Delta}}{6}s + C_2\right) + \cdots \quad \text{as } s \to +\infty.$$

We also have for $r \to +\infty$,

$$U(r) \sim r^{\frac{2+\alpha}{3}}\left(\frac{9}{(2+\alpha)(3N+\alpha-4)}\right)^{\frac{1}{3}} + \delta_1 r^{-\frac{N-2}{2}}\cos\left(\frac{\sqrt{-\Delta}}{6}\ln r + C_2\right) + \cdots, \tag{1.54}$$

and from the fact that $\lambda = \gamma^{2+\alpha}/U^3(\gamma)$ we get again that

$$\lambda \sim \lambda_* = \frac{(2+\alpha)(3N+\alpha-4)}{9} \quad \text{as } \gamma \to \infty.$$

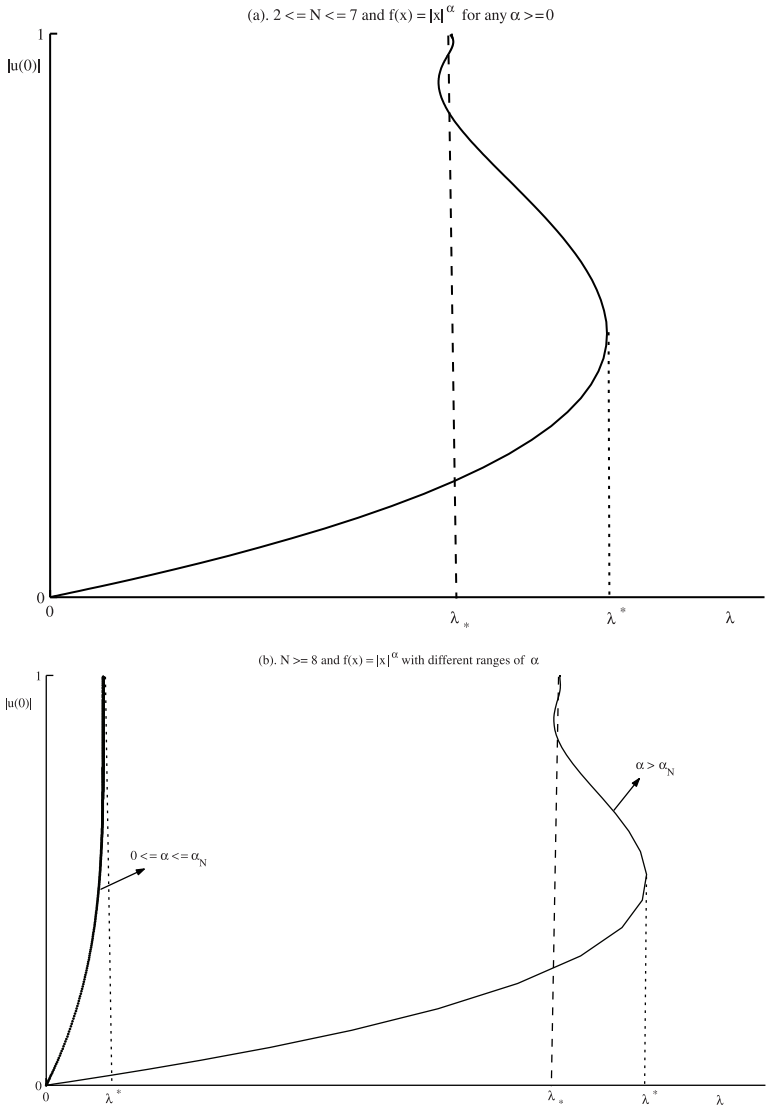

FIGURE 1.5. Top: Plots of $u(0)$ versus λ for $2 \leq N \leq 7$, where $u(0)$ oscillates around the value λ_* defined in (1.52) and u^* is regular. Bottom: Plots of $u(0)$ versus λ for $N \geq 8$: when $0 \leq \alpha \leq \alpha_N$, there exists a unique solution for $(S)_\lambda$ with $\lambda \in (0, \lambda^*)$ and u^* is singular; when $\alpha > \alpha_N$, $u(0)$ oscillates around the value λ_* defined in (1.52) and u^* is regular.

Note the oscillatory behavior of $U(r)$ in (1.54) for large r, which means that λ is expected to oscillate around the value $\lambda_* = \frac{(2+\alpha)(3N+\alpha-4)}{9}$ and $u_\gamma(0) \uparrow 1$ as

$\gamma \to \infty$. The diagrams above point to the existence of a sequence $\{\lambda_i\}$ satisfying

$$\lambda_0 = 0, \quad \lambda_{2k} \nearrow \lambda_* \quad \text{as } k \to \infty,$$
$$\lambda_1 = \lambda^*, \quad \lambda_{2k-1} \searrow \lambda_* \quad \text{as } k \to \infty,$$

such that exactly $2k+1$ solutions for $(S_{\lambda,\alpha})$ exist when $\lambda \in (\lambda_{2k}, \lambda_{2k+2})$, while there are exactly $2k$ solutions when $\lambda \in (\lambda_{2k+1}, \lambda_{2k-1})$. Furthermore, $(S_{\lambda,\alpha})$ has infinitely many solutions at $\lambda = \lambda_*$. The three cases (1.53a), (1.53b), and (1.53c) considered here for N and α are illustrated by the diagrams in Figure 1.4, Figure 1.5(a), and Figure 1.5(b), respectively.

We now infer from the above that the bifurcation diagrams show four possible regimes—at least if the domain is a ball:

VII. There is exactly one branch of solutions for $0 < \lambda < \lambda^*$. This regime occurs when $N \geq 8$ and $0 \leq \alpha \leq \alpha_N = \frac{3N-14-4\sqrt{6}}{4+2\sqrt{6}}$. The above observations actually show that in this range, the first branch of solutions "disappears" at λ^*, which happens to be equal to $\lambda_*(\alpha, N) = \frac{(2+\alpha)(3N+\alpha-4)}{9}$.

VIII. There exists an infinite number of branches of solutions. This regime occurs when
- $N = 1$ and $\alpha \geq \alpha_1 = -\frac{1}{2} + \frac{3}{4}\sqrt{6}$;
- $2 \leq N \leq 7$ and $\alpha \geq 0$;
- $N \geq 8$ and $\alpha > \alpha_N$.

In this case, $\lambda_*(\alpha, N) < \lambda^*$ and the multiplicity becomes arbitrarily large as λ approaches—from either side—$\lambda_*(\alpha, N)$, at which there is a touchdown solution u (i.e., $\|u\|_\infty = 1$).

IX. There exists a finite number of branches of solutions. In this case, we have again that $\lambda_*(\alpha, N) < \lambda^*$, but now the branch approaches the value 1 monotonically, and the number of solutions increases but remains finite as λ approaches $\lambda_*(\alpha, N)$. This regime occurs when $N = 1$ and $1 < \alpha \leq \alpha_1$.

X. There exist exactly two branches of solutions for $0 < \lambda < \lambda^*$ and one solution for $\lambda = \lambda^*$. The bifurcation diagram disappears when it returns to $\lambda = 0$. This regime occurs when $N = 1$ and $0 \leq \alpha \leq 1$.

1.4.2. Asymptotic Analysis of Dynamic Quenching Profiles. Consider now the dynamic problem $(D_{\lambda,f})$ on a domain Ω. Numerical evidence shows that for small voltages λ, a solution exists for all time and eventually converges to the corresponding minimal solution of the stationary equation. On the other hand, for large voltages λ, the solution must quench (i.e., touch the ground plate) at a finite time $T_\lambda(\Omega, f)$. This naturally leads to the following queries:

XI. Is the pull-in voltage λ^* the exact cutoff between a regime of globally convergent solutions, and the one where we have quenching in finite time? Moreover, what is the mode of deflection when $\lambda = \lambda^*$, and can we have quenching in infinite time?

XII. Estimate the quenching time $T_\lambda(\Omega, f)$ in terms of the geometry of the domain, the permittivity profile f, and the excess voltage $\lambda - \lambda^*$.

Besides the qualitative behavior of the solutions for various λ, and the estimates on the quenching time $T_\lambda(\Omega, f)$, one is also interested in describing the quenching profile of the deflection, including the information on quenching rates as well as quenching locations and how they are affected by the permittivity. With this in mind, we now use elementary asymptotic analysis to identify the issues and the facts that need to be established. We start with the simplest case.

Quenching Profile When $f(x) \equiv 1$. We also assume that quenching occurs at $x = 0$ and $t = T$. In the absence of diffusion, the time-dependent behavior of solutions for $(D_{\lambda,1})$ is given by $u_t = \lambda(1-u)^{-2}$. Integrating this differential equation and setting $u(T) = 1$, we get $(1-u)^3 = -3\lambda(t-T)$. This solution motivates the introduction of a new variable $v(x,t)$ defined by

$$v = \frac{1}{3\lambda}(1-u)^3. \tag{1.55}$$

A simple calculation shows that $(D_{\lambda,1})$ transforms to the following problem for v:

$$v_t = \Delta v - \frac{2}{3v}|\nabla v|^2 - 1, \quad x \in \Omega,\ t > 0; \tag{1.56a}$$

$$v(x,k) = \frac{1}{3\lambda} \qquad \text{on } (\partial\Omega \times (0,+\infty)) \cup (\Omega \times \{0\}). \tag{1.56b}$$

Notice that $u = 1$ maps to $v = 0$. We will find a formal power series for a radially symmetric solution to (1.56a) near $v = 0$, in the form

$$v(x,t) = v_0(t) + \frac{r^2}{2!}v_2(t) + \frac{r^4}{4!}v_4(t) + \cdots, \tag{1.57}$$

where $r = |x|$. We then substitute (1.57) into (1.56a) and collect coefficients in r. In this way, we obtain the following coupled ordinary differential equations for v_0 and v_2:

$$v_0' = -1 + Nv_2, \quad v_2' = -\frac{4}{3v_0}v_2^2 + \frac{(N+2)}{3}v_4. \tag{1.58}$$

We are interested in the solution to this system for which $v_0(T) = 0$, with $v_0' < 0$ and $v_2 > 0$ for $T - t > 0$ with $T - t \ll 1$. System (1.58) has a closure problem in that v_2 depends on v_4. However, we will assume that $v_4 \ll v_2^2/v_0$ near the singularity. With this assumption, (1.58) reduces to

$$v_0' = -1 + Nv_2, \quad v_2' = -\frac{4}{3v_0}v_2^2. \tag{1.59}$$

We now solve system (1.59) asymptotically as $t \to T^-$. We first assume that $Nv_2 \ll 1$ near $t = T$. This leads to $v_0 \sim T - t$, and the following differential equation for v_2:

$$v_2' \sim \frac{-4}{3(T-t)}v_2^2 \quad \text{as } t \to T^-. \tag{1.60}$$

By integrating (1.60), we obtain that

$$v_2 \sim -\frac{3}{4[\log(T-t)]} + \frac{B_0}{[\log(T-t)]^2} + \cdots \quad \text{as } t \to T^- \tag{1.61}$$

for some unknown constant B_0. From (1.61), we observe that the consistency condition that $Nv_2 \ll 1$ as $t \to T^-$ is indeed satisfied. Substituting (1.61) into the equation (1.59) for v_0, we obtain for $t \to T^-$ that

$$v_0' = -1 + N\left(-\frac{3}{4[\log(T-t)]} + \frac{B_0}{[\log(T-t)]^2} + \cdots\right). \tag{1.62}$$

Using the method of dominant balance, we look for a solution to (1.62) as $t \to T^-$ in the form

$$v_0 \sim (T-t) + (T-t)\left[\frac{C_0}{[\log(T-t)]} + \frac{C_1}{[\log(T-t)]^2} + \cdots\right] \tag{1.63}$$

for some C_0 and C_1 to be found. A simple calculation yields that

$$v_0 \sim (T-t) + \frac{-3N(T-t)}{4|\log(T-t)|} + \frac{-N(B_0 - \frac{3}{4})(T-t)}{|\log(T-t)|^2} + \cdots \quad \text{as } t \to T^-. \tag{1.64}$$

The local form for v near quenching is $v \sim v_0 + r^2 v_2/2$. Using the leading term in v_2 from (1.61) and the first two terms in v_0 from (1.64), we obtain the local form

$$v \sim (T-t)\left[1 - \frac{3N}{4|\log(T-t)|} + \frac{3r^2}{8(T-t)|\log(T-t)|} + \cdots\right] \tag{1.65}$$

for $r \ll 1$ and $t - T \ll 1$. Finally, using the relation (1.55) between u and v, we conclude that

$$u \sim 1 - [3\lambda(T-t)]^{\frac{1}{3}}\left(1 - \frac{3N}{4|\log(T-t)|} + \frac{3r^2}{8(T-t)|\log(T-t)|} + \cdots\right)^{\frac{1}{3}}. \tag{1.66}$$

An important question is then:

XIII. To what extent does (1.66) describe the profile of a quenching solution, and how valid is this description for general permittivities?

Before going further, we note that numerical experiments can be performed thanks to the following observation, which will also have a theoretical relevance as well. Indeed, we observe that if we use the local behavior $v \sim (T-t) + 3r^2/[8|\log(T-t)|]$, we get that

$$\frac{|\nabla v|^2}{v} \sim \left[\frac{2}{3}|\log(T-t)| + \frac{16(T-t)|\log(T-t)|^2}{9r^2}\right]^{-1}. \tag{1.67}$$

Hence, the term $|\nabla v|^2/v$ in (1.56a) is bounded for any r, even as $t \to T^-$. This allows us to use a simple finite-difference scheme to compute numerical solutions for the transformed problem (1.56).

For the slab domain $(-\frac{1}{2}, \frac{1}{2})$, we define v_j^m for $j = 1, \ldots, N+2$ to be the discrete approximation to $v(m\Delta t, -\frac{1}{2} + (j-1)h)$, where $h = \frac{1}{N+1}$ and Δt are the

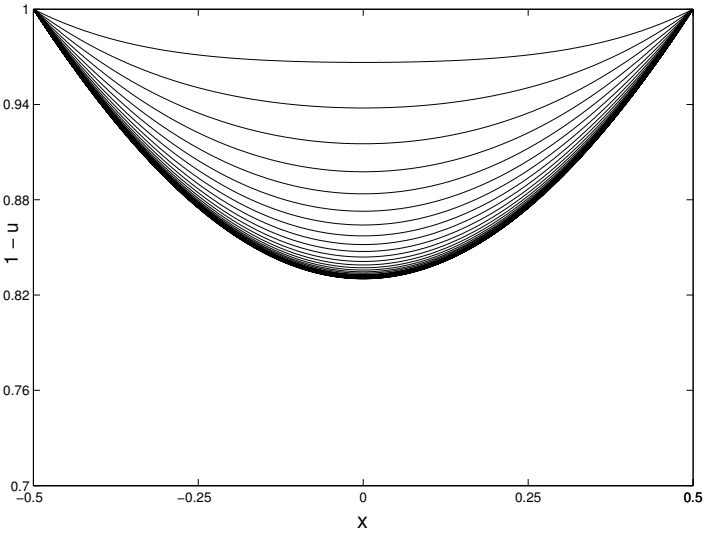

FIGURE 1.6. Plots of $1-u(x,t)$ versus x with $\lambda = 1$ at different times. Here it is observed that the dynamic solution approaches a steady state as the time t is increased.

spatial and temporal mesh sizes, respectively. A second-order accurate-in-space, and a first-order accurate-in-time discretization of (1.56) is

$$v_j^{m+1} = v_j^m + \Delta t\left(\frac{(v_{j+1}^m - 2v_j^m + v_{j-1}^m)}{h^2} - 1 - \frac{(v_{j+1}^m - v_{j-1}^m)^2}{6v_j^m h^2}\right), \quad j = 2,\ldots,N+1, \tag{1.68}$$

with $v_1^m = v_{N+2}^m = (3\lambda)^{-1}$ for $m \geq 0$. The initial condition is $v_j^0 = (3\lambda)^{-1}$ for $j = 1,\ldots,N+2$. The time step Δt is chosen to satisfy $\Delta t < h^2/4$ for the stability of the discrete scheme. Using this argument, one can get useful numerical results for the dynamic deflection u; see Figures 1.6, 1.7, and 1.8.

Quenching Profile for a Variable Permittivity. Suppose we are now dealing with a spatially variable permittivity profile in a slab domain. Let u again be a quenching solution of $(D_{\lambda,f})$ at finite time T, and let $x = x_0$ be a quenching point of u. With the transformation

$$v = \frac{1}{3\lambda}(1-u)^3, \tag{1.69}$$

problem $(D_{\lambda,f})$ in the slab domain transforms to

$$v_t = v_{xx} - \frac{2}{3v}v_x^2 - f(x), \quad -\frac{1}{2} < x < \frac{1}{2},\ t > 0, \tag{1.70a}$$

$$v = \frac{1}{3\lambda},\ x = \pm\frac{1}{2}; \quad v = \frac{1}{3\lambda},\ t = 0, \tag{1.70b}$$

where $f(x)$ is the permittivity profile.

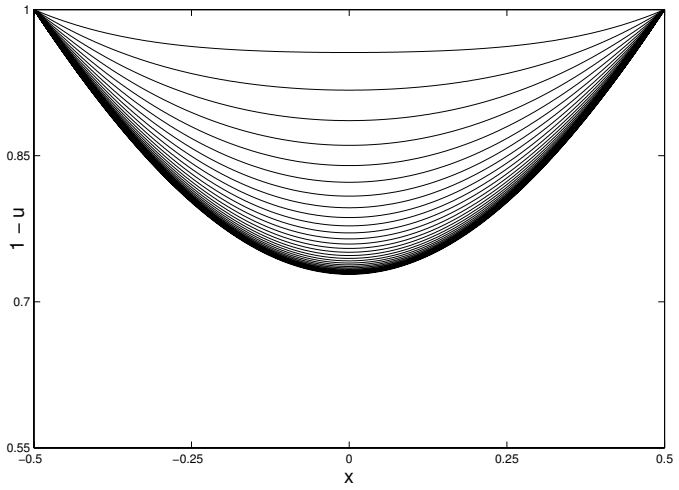

FIGURE 1.7. Plots of $1 - u(x,t)$ versus x with $\lambda = 1.3$ at different times. Here it is observed that the dynamic solution approaches a steady state as the time t is increased.

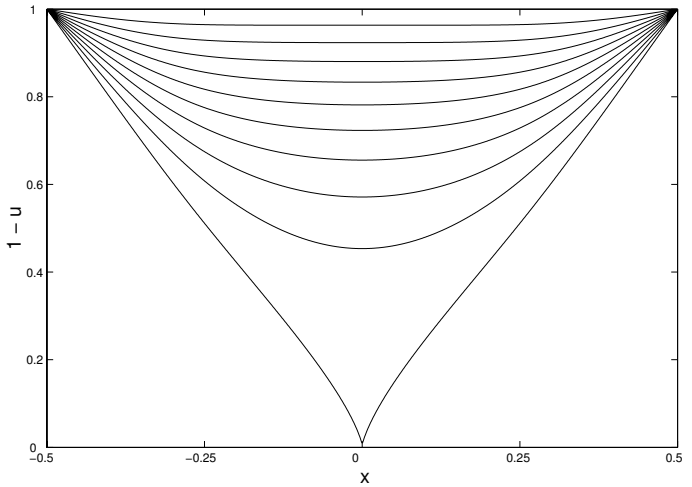

FIGURE 1.8. Plots of $1-u(x,t)$ versus x with $\lambda = 6$ at different times. Here the quenching behavior is observed at finite time.

Look now for a quenching profile for (1.70) near $x = x_0$ at time T in the form

$$v(x,t) = v_0(t) + \frac{(x-x_0)^2}{2!}v_2(t) + \frac{(x-x_0)^3}{3!}v_3(t) + \frac{(x-x_0)^4}{4!}v_4(t) + \cdots . \tag{1.71}$$

In order for v to be a quenching profile, it is clear that we must require

$$\lim_{t\to T^-} v_0 = 0, \quad v_0 > 0 \quad \text{for } t < T, \qquad v_2 > 0 \quad \text{for } t - T \ll 1. \tag{1.72}$$

We first discuss the case where $f(x)$ is analytic at $x = x_0$ with $f(x_0) > 0$. Therefore, for $x - x_0 \ll 1$, f itself has the convergent power series expansion

$$f(x) = f_0 + f_0'(x - x_0) + \frac{f_0''(x - x_0)^2}{2} + \cdots, \tag{1.73}$$

where $f_0 := f(x_0)$, $f_0' = f'(x_0)$, and $f_0'' := f''(x_0)$. Substituting (1.71) and (1.73) into (1.70), we equate the powers of $x - x_0$ to obtain

$$v_0' = -f_0 + v_2, \tag{1.74a}$$

$$v_2' = -\frac{4v_2^2}{3v_0} + v_4 - f_0'', \tag{1.74b}$$

$$v_3 = f_0'. \tag{1.74c}$$

We now assume that $v_2 \ll 1$ and $v_4 \ll 1$ as $t \to T^-$. This yields that $v_0 \sim f_0(T - t)$, and

$$v_2' \sim -\frac{4v_2^2}{3f_0(T - t)} - f_0''. \tag{1.75}$$

For $t \to T^-$, we obtain from a simple dominant balance argument that

$$v_2 \sim -\frac{3f_0}{4[\log(T - t)]} + \cdots \quad \text{as } t \to T^-. \tag{1.76}$$

Substituting (1.76) into (1.74a) and integrating, we obtain that

$$v_0 \sim f_0(T - t) + \frac{-3f_0(T - t)}{4|\log(T - t)|} + \cdots \quad \text{as } t \to T^-. \tag{1.77}$$

Next, we substitute (1.76), (1.77), and (1.74c) into (1.71) to obtain the local quenching behavior

$$v \sim f_0(T - t)\left[1 - \frac{3}{4|\log(T - t)|} + \frac{3(x - x_0)^2}{8(T - t)|\log(T - t)|} + \frac{f_0'(x - x_0)^3}{6f_0(T - t)} + \cdots\right], \tag{1.78}$$

for $(x - x_0) \ll 1$ and $t - T \ll 1$. Finally, using the relation (1.69) between u and v, we conclude that

$$u \sim 1 - [3f(x_0)\lambda(T - t)]^{\frac{1}{3}} \cdot \left(1 - \frac{3}{4|\log(T - t)|} + \frac{3(x - x_0)^2}{8(T - t)|\log(T - t)|} + \frac{f'(x_0)(x - x_0)^3}{6f_0(T - t)} + \cdots\right)^{\frac{1}{3}}. \tag{1.79}$$

This formal analysis is obviously not satisfactory if the quenching point x_0 happens to be a zero of the profile f (i.e., if $f(x_0) = 0$), and leads to the following important question:

XIV. Can finite-time quenching occur at the zero set of permittivity profile f?

Again, formal asymptotic analysis points towards a negative answer to this question by showing how to exclude the possibility that $f(x_0) = 0$. Indeed, assume $f(x)$ is analytic at $x = x_0$, with $f(x_0) = 0$ and $f'(x_0) = 0$, so that $f(x) = a_0(x - x_0)^2 + O((x - x_0)^3)$ as $x \to x_0$ with $a_0 > 0$. We then look for a power series solution to (1.70) as in (1.71). In place of (1.74) for v_3, we get $v_3 = 0$, and

$$v_0' = v_2, \quad v_2' = -\frac{4v_2^2}{3v_0} + v_4 - 2a_0. \tag{1.80}$$

Assuming that $v_4 \ll 1$ as before, we can combine the equations in (1.80) to get

$$v_0'' = -\frac{4(v_0')^2}{3v_0} - 2a_0. \tag{1.81}$$

By solving (1.81) with $v_0(T) = 0$, we obtain the exact solution

$$v_0 = -\frac{3a_0}{11}(T - t)^2 < 0, \quad v_2 = \frac{6a_0}{11}(T - t). \tag{1.82}$$

Since the criteria (1.72) are not satisfied, the form (1.82) does not represent a quenching profile centered at $x = x_0$. Therefore, the above asymptotical analysis also shows that the point $x = x_0$ satisfying $f(x_0) = 0$ is not a quenching point of u.

1.4.3. Evidence and Conjectures for Fourth-Order MEMS Models. The case where the rigidity is not neglected leads to a substantial number of mathematical challenges. The equation is then of the fourth order in space and one has to deal with the biharmonic operator, which is not as well understood mathematically as the Laplacian. For one, Δ^2 does not satisfy the maximum principle on general domains when we are dealing with the physically relevant clamped boundary conditions. However, if the domain is a ball where Δ^2 satisfies a comparison principle and minimal solutions are radially symmetric, numerical and analytical evidence points towards a strong analogy with the corresponding second-order model, provided we increase all critical dimensions by 1. Specifically, the following picture emerges for equation $(C_{\lambda,1})$, at least when Ω is a ball:

There exists again a *pull-in voltage* $\lambda^* > 0$ such that (C_λ) has at least one solution if $\lambda < \lambda^*$, while it has none if $\lambda > \lambda^*$. However, the dependence of the bifurcation diagrams on the dimension changes as follows:

XV. In dimensions 1 and 2 there exist exactly two branches of solutions for $0 < \lambda < \lambda^*$ and one solution for $\lambda = \lambda^*$. The second (unstable) solution heads towards a quenching state when the bifurcation diagram returns to $\lambda = 0$.

XVI. There exists at most one solution at λ^* in any dimension, while the uniqueness of solutions also occurs at small voltages λ whenever $N \geq 3$.

XVII. In dimensions $3 \leq N \leq 8$ there exist exactly two solutions for λ in a small left neighborhood of λ^*, as well as a curve $(\lambda(t), u(t))_{t \geq 0}$ in the

solution set

$$\mathcal{V} = \{(\lambda, u) \in (0, +\infty) \times C^2(\bar{\Omega}) : u \text{ is a solution of } (C_{\lambda,1})\}, \tag{1.83}$$

starting from $(0, 0)$ at $t = 0$ with $\|u(t)\|_\infty \to 1$ as $t \to +\infty$, while having infinitely many turning points.

XVIII. Describe the situation in more general domains.

Queries I to XVIII and many more will be addressed throughout this monograph under various levels of generality.

1.5. Brief Outline

This text is divided into three major parts. The first one covers the simplest situation, which deals with the stationary case when one ignores bending. The results here are the most satisfying from the mathematical point of view. The stationary case for a nonelastic model is dealt with in Part III, where the results are satisfactory only in the case of a radially symmetric domain. The dynamic model is covered in Part II, but only in the parabolic case where we ignore rotational inertia, which would have given the equation a hyperbolic character.

Part I: Second-Order Equations with Singular Nonlinearities Modeling Stationary MEMS. This part deals with the stationary deflection of an elastic membrane satisfying the elliptic problem $(S_{\lambda,f})$, where $\lambda > 0$ represents the applied voltage. The nonnegative function $f(x)$ will describe the varying permittivity profile of the elastic membrane, which will be allowed to vanish somewhere, but will always be assumed to satisfy

$$f \in C^\beta(\bar{\Omega}) \quad \text{for some } \beta \in (0, 1],\ 0 \le f \le 1, \text{ and } f \not\equiv 0. \tag{1.84}$$

Chapter 2. We start by considering the *pull-in voltage* for $(S_{\lambda,f})$, which is defined as

$$\lambda^*(\Omega, f) = \sup\{\lambda > 0 \mid (S_{\lambda,f}) \text{ possesses at least one solution}\}. \tag{1.85}$$

Our goal is to establish the basic properties of the pull-in voltage λ^* and to analyze its dependence on the size and the shape of the domain, as well as on the permittivity profile.

Chapter 3. We study the branch $\lambda \mapsto u_\lambda$ of *minimal solutions* for $(S_{\lambda,f})$, i.e., those that are below any other solution. We include a detailed analysis of the monotonicity, differentiability, and compactness properties of this branch with respect to the voltage λ. The stability and regularity properties of such minimal solutions are also investigated, with a particular emphasis on the extremal solution, i.e., the one that corresponds to the pull-in voltage λ^*. The results confirm the complexity and richness of the problem and its dependence on the dimension of the ambient space and on the permittivity profile, as suggested by the bifurcation diagrams (Figures 1.3–1.5). In particular, there is a critical dimension ($N = 7$) below which all minimal solutions—including the solution at the pull-in voltage u_{λ^*}—are regular, while u_{λ^*} may "touch the plate" (i.e., $u_{\lambda^*}(x) = 1$ at some point $x \in \Omega$) for dimension $N \ge 8$.

On the other hand, a closer study of the minimal branch for powerlike profiles on the unit ball uncovers a new and interesting phenomenon: certain permittivity profiles can restore compactness and regularity to the problem at the pull-in voltage. This analysis is done through a blowup procedure that we introduce in this chapter, but which we will explore more deeply in the following ones.

Chapter 4. One of the primary goals in the design of MEMS devices is to optimize the pull-in distance over a certain allowable voltage range that is set by the power supply. Here the *pull-in distance* refers to the maximum stable deflection of the elastic membrane before quenching occurs. It will be denoted by $P(\Omega, f, N)$. Since the L^∞-norm of the minimal solutions u_λ for $(S_{\lambda,f})$ is strictly increasing in λ, the pull-in distance is achieved exactly at $\lambda = \lambda^*$, that is $P(\Omega, f, N) = \|u^*\|_{L^\infty(\Omega)}$, where u^* is the unique extremal steady state of $(S_{\lambda,f})$. Our first goal in this chapter is to give upper and lower bounds for $P(\Omega, f, N)$ in terms of the permittivity f, the dimension N, and the geometry of the domain. We also study the effect of powerlike permittivity profiles $f(x) = |x|^\alpha$ and the dimension N on both the pull-in voltage and the pull-in distance. In particular, we give rigorous proofs that explain various numerically observed phenomena, such as the curious fact noted in [**99**], that on a two-dimensional disk, a change in the power law has no effect on the pull-in distance, as well as the "rule of thumb" that the pull-in distance is about one-third the size of the zero voltage gap [**140**, p. 214].

Chapter 5. We continue the analysis of problem $(S_{\lambda,f})$ by considering the linearized operator $L_{u,\lambda} = -\Delta - 2\lambda f(x)/(1-u)^3$, at a solution u, and its eigenvalues $\{\mu_{k,\lambda}(u); k = 1, 2, \dots\}$, the first one of which is simple and given by

$$\mu_{1,\lambda}(u) = \inf\left\{\langle L_{u,\lambda}\phi, \phi\rangle_{L^2(\Omega)} : \phi \in C_0^\infty(\Omega), \int_\Omega \phi^2\, dx = 1\right\}. \tag{1.86}$$

When the infimum is attained at a first, positive eigenfunction ϕ_1, the second eigenvalue is then given by the formula

$$\mu_{2,\lambda}(u) = \inf\left\{\langle L_{u,\lambda}\phi, \phi\rangle_{L^2(\Omega)} : \phi \in C_0^\infty(\Omega), \int_\Omega \phi^2\, dx = 1, \text{and} \int_\Omega \phi\phi_1\, dx = 0\right\}. \tag{1.87}$$

This construction can be iterated to obtain the k^{th} eigenvalue $\mu_{k,\lambda}(u)$ with the convention that eigenvalues are repeated according to their multiplicities [**23**]. The Morse index $m(u, \lambda)$ of a solution u is the largest k for which $\mu_{k,\lambda}(u)$ is negative.

The compactness—in dimensions $1 \le N \le 7$—of the minimal branch of semistable solutions, i.e., those with zero Morse index (or those verifying $\mu_{1,\lambda}(u) \ge 0$), gives rise to a second unstable solution U_λ of $(S_{\lambda,f})$ for λ in a small deleted left neighborhood of λ^*. We give a "mountain pass" variational construction of this second solution for λ close to λ^* whenever the minimal branch is compact. We then establish, in the right dimensions, the compactness of this first branch of unstable solutions whose Morse index is equal to 1, i.e., those such that

$$\mu_{1,\lambda}(u) < 0 \quad \text{but} \quad \mu_{2,\lambda}(u) \ge 0. \tag{1.88}$$

This eventually leads to the identification of a second bifurcation point. The main tool here for controlling the blowup behavior of a possible noncompact sequence

of solutions is a linear instability result which states that there is no stable solution for the limiting problem (on $\mathbb{R}^N$) if either $1 \leq N \leq 7$ or if $N \geq 8$ and $\alpha > \alpha_N$. Roughly speaking, compactness is deduced from the fact that a blown-up sequence of solutions whose Morse indices do not exceed 1 cannot account for such instability at infinity.

Chapter 6. We investigate here the extent to which the properties of the global set of solutions—as illustrated in the bifurcation diagram of Figure 1.3—can be established mathematically in more general situations. We start by extending the results of the previous chapters and establishing the compactness of any set of solutions of $(S_{\lambda,f})$, provided their Morse indices are uniformly bounded and not just equal to 0 as in Chapter 3 or less than or equal to 1 as in Chapter 4. The result will again be true for dimensions $2 \leq N \leq 7$ and for permittivity profiles f of the form (1.42). This will follow from a detailed blowup analysis of noncompact sequences of solutions, combined with a result stating that a solution u of finite Morse index is either regular or "badly singular," meaning that the set $\{x \in \Omega : u(x) = 1\}$ has no isolated points. As a by-product, we show the existence of a quenching branch of solutions with an infinite number of turns (i.e., solutions with arbitrarily large Morse indices) as long as the extremal solution u_{λ^*} is a classical solution, and in particular for dimensions $2 \leq N \leq 7$. On the other hand, we show a uniqueness result for small voltage in the case of power-law profiles—without any restriction on the energy or on the Morse index—provided the domain Ω is star-shaped and $N \geq 3$, or when it is strictly convex (or suitably symmetric) in the two-dimensional case.

Chapter 7. We consider in this chapter the particular case of a MEMS device with a power-law profile and whose domain satisfies various symmetry conditions. More information about the set of solutions can be given in this situation, which is still complex—even in the radially symmetric case—as shown in the above bifurcation diagrams.

Our main purpose here, however, is to introduce mathematical techniques that have not been used so far. The first section includes an interesting and nonstandard one-dimensional Sobolev inequality. This will be followed by a powerful monotonicity formula that should have many applications. Section 3 deals with the counterpart of the last chapter's compactness result in the case of radially symmetric solutions, where the role of the radial Morse indices is investigated. This will allow for a more detailed description of the branches of radially symmetric solutions that closely reflects the numerical evidence. We finally pay special attention to the two-dimensional case, which arguably is the most relevant for engineering applications.

Part II: Parabolic Equations with Singular Nonlinearities Modeling MEMS Dynamic Deflections. The second part of this monograph is devoted to the study of dynamic deflection of $(D_{\lambda,f})$. We note that the case when the permittivity profile $f(x) \equiv 1$ was studied in the 1980s (see [**95, 96**] and references therein). However, the case of a varying and somewhere vanishing profile turned out to be a rich source of new and interesting mathematical phenomena.

Chapter 8. It is shown here that whenever $\lambda \leq \lambda^*(\Omega, f)$, the unique solution u of $(D_{\lambda,f})$ exists for all time and must globally converge as $t \to +\infty$ to its corresponding unique minimal steady state. On the other hand, if $\lambda > \lambda^*(\Omega, f)$ the unique solution u of $(D_{\lambda,f})$ must quench at finite time $T_\lambda(\Omega, f)$ in the sense that $u(x,t)$ reaches 1 at time $T_\lambda(\Omega, f)$.

We also study the set of finite-time quenching points, and we show among other things that generically they cannot occur at zero points of the varying permittivity profile $f(x)$, a fact first observed numerically and conjectured in [**99**]. We then study the case of convex domains and also the particular case of radially symmetric solutions on the ball, where often the only location of finite-time quenching points is at the origin.

Chapter 9. We analyze and estimate the finite quenching time $T_\lambda(\Omega, f)$ of the dynamic solutions of $(D_{\lambda,f})$. This often translates into useful information concerning the speed of the operation for many MEMS devices, such as RF switches and microvalves. We start by giving comparison results for the quenching time $T_\lambda(\Omega, f)$ in terms of the profile f and the voltage λ. We then obtain various analytic estimates for quenching times for large voltages λ, while in the third section we give analytic and numerical estimates on the quenching time for any λ above the pull-in voltage λ^*. The last section deals with the particular but important case when the extremal steady state is regular, which occurs at least in low dimensions $(1 \leq N \leq 7)$.

Chapter 10. The focus here is on the quenching profiles of the dynamic solutions of $(D_{\lambda,f})$, when λ exceeds the pull-in voltage λ^*. Since such solutions must quench at a finite time $T = T_\lambda(\Omega, f)$, we obtain—by adapting self-similarity methods and center manifold analysis—estimates on the quenching rate and a relatively precise description of the solution near time T and around a given quenching point a. Under a compactness assumption on the quenching set, we establish energy quenching rates such as

$$\varliminf_{t \to T^-} \int_\Omega \frac{f(x)}{(1-u(x,t))^\gamma}\, dx = +\infty \tag{1.89}$$

for any $\gamma > \frac{3}{2}N$. On the other hand, we show that in the radially symmetric case, a solution quenching at 0 must do so in such a way that for any $C > 0$,

$$\lim_{t \to T^-} \frac{1-u(x,t)}{(T-t)^{\frac{1}{3}}} = (3\lambda f(0))^{\frac{1}{3}} \tag{1.90}$$

uniformly on $|x| \leq C\sqrt{T-t}$.

More precise quenching behavior is given in dimension $N = 1$. For example, it is shown that for sufficiently large voltage λ, finite-time quenching necessarily occurs near the maximum points of the profile f, which refines considerably the results obtained in Chapter 8 about finite-time quenching not occurring at the zero points of the permittivity profile f.

Part III: Fourth-Order Equations Modeling Nonelastic MEMS. The third part of this monograph is devoted to the study of nonelastic MEMS models where

bending effects are taken into consideration. Specifically, we shall consider equation $(C_{\lambda,f})$ where we suppose a clamped boundary condition, as well as $(P_{\lambda,f})$ where a pinned boundary is assumed.

Chapter 11. We study here the fourth-order nonlinear boundary value problem $\Delta^2 u = \frac{\lambda}{(1-u)^2}$ on a ball $B \subset \mathbb{R}^N$, again under Dirichlet boundary conditions $u = \frac{\partial u}{\partial \eta} = 0$ on ∂B; there exists $\lambda^* > 0$ such that for $\lambda \in (0, \lambda^*)$, the equation has a minimal (classical) solution u_λ that satisfies $0 < u_\lambda < 1$. For $\lambda > \lambda^*$ there are no solutions of any kind. In the extremal case $\lambda = \lambda^*$; we prove the existence of a weak solution that has finite energy and that is the unique solution even in a very weak sense. The main result asserts that the extremal solution u_{λ^*} is regular $(\sup_B u_{\lambda^*} < 1)$ provided $N \leq 8$, while u_{λ^*} is singular $(\sup_B u_{\lambda^*} = 1)$ for $N \geq 9$, in which case $1 - C_0|x|^{4/3} \leq u_{\lambda^*}(x) \leq 1 - |x|^{4/3}$ on the unit ball, where

$$C_0 := \left(\frac{\lambda^*}{\bar{\lambda}}\right)^{\frac{1}{3}} \quad \text{and} \quad \bar{\lambda} := \frac{8(N-\frac{2}{3})(N-\frac{8}{3})}{9}.$$

Estimates on λ^*, as well as stability properties of minimal solutions, are also established.

Chapter 12. We consider here the fourth-order nonlinear equation $B\Delta^2 u - T\Delta u = \frac{\lambda}{(1-u)^2}$ on a bounded smooth domain $\Omega \subset \mathbb{R}^N$, with the Navier boundary conditions $u = \Delta u = 0$ on $\partial\Omega$, and where $\lambda > 0$ is a parameter, and $T > 0$ and $B > 0$ are fixed constants. There again exists a well-defined pull-in voltage $\lambda^* > 0$ such that for $\lambda < \lambda^*$, there is a branch of minimal solutions that are also stable. The minimal solution is unique at $\lambda = \lambda^*$ and is regular in dimensions $N \leq 4$. The novelty here is that, unlike the case when $B = 0$, there exists, at least on a two-dimensional convex smooth domain, a second mountain pass solution for all $\lambda \in (0, \lambda^*)$, which shows that the two-dimensional bifurcation diagram of (P_λ) changes drastically when $B > 0$. The asymptotic behavior of the second solution as $\lambda \to 0$ is also studied. The situation is again much clearer on a radially symmetric domain where the extremal solution u_{λ^*} is regular $(\sup_B u_{\lambda^*} < 1)$ provided $N \leq 8$, while u_{λ^*} is singular $(\sup_B u_{\lambda^*} = 1)$ for $N \geq 9$ and $\frac{T}{B}$ is small enough. Key ingredients for proving the singularity of the extremal solution in higher dimensions (above $N = 9$) are the new Hardy-Rellich inequalities described in the Appendix.

Glossary of Notation. The following list of notation and abbreviations will be used throughout this book. Let Ω be a smooth domain of $\mathbb{R}^n$.

- $C^\infty(\Omega, \mathbb{R}^n)$ (resp., $C_0^\infty(\Omega, \mathbb{R}^n)$) will denote the space of infinitely differentiable functions (resp., the space of infinitely differentiable functions with compact support) on Ω.
- For $1 \leq p < +\infty$, $L^p(\Omega)$ will be the space of all integrable functions $u : \Omega \to \mathbb{R}$ with norm

$$\|u\|_p = \left(\int_\Omega |u(x)|^p \, dx\right)^{\frac{1}{p}}.$$

For $p = +\infty$, $L^\infty(\Omega)$ will be the space of all measurable functions $u : \Omega \to \mathbb{R}$ such that

$$\|u\|_\infty = \operatorname{ess\,sup} \lim_{x \in \Omega} |u(x)| < +\infty.$$

- For $m \in \mathbb{N}$ and $1 \leq p \leq +\infty$, $W^{m,p}(\Omega)$ will be the Banach space of (classes of) measurable functions $u : \Omega \to \mathbb{R}$ such that $D^\alpha u \in L^p(\Omega)$ in the sense of distributions, for every multi-index α with $|\alpha| \leq m$. The space $W^{m,p}(\Omega)$ will be equipped with the norm

$$\|u\|_{W^{m,p}(\Omega)} = \sum \lim_{|\alpha| \leq m} \|D^\alpha u\|_p.$$

  $W_0^{m,p}(\Omega)$ will be the closure of $C_0^\infty(\Omega, \mathbb{R})$ in $W^{m,p}(\Omega)$, and $W^{-m,q}(\Omega)$ will denote the Banach space dual of $W_0^{m,p}(\Omega)$, where $\frac{1}{p} + \frac{1}{q} = 1$.
- $W^{m,2}(\Omega)$ (resp., $W_0^{m,2}(\Omega)$) will be denoted by $H^m(\Omega)$ (resp., $H_0^m(\Omega)$). They will be Hilbert spaces once equipped with the scalar product

$$\langle u, v \rangle = \int_\Omega u(x)v(x)dx.$$

  The dual of $H_0^{-m}(\Omega)$ will be denoted by $H^{-m}(\Omega)$.